SEM/EDX, XPS, AND IMPEDANCE SPECTROSCOPY OF LiFePO$_4$ AND LiFePO$_4$/C CERAMICS

A.F. Orliukas [a], **K.-Z. Fung** [b], **V. Venckutė** [a], **V. Kazlauskienė** [c], **J. Miškinis** [c], **A. Dindune** [d],

Z. Kanepe [d], **J. Ronis** [d], **A. Maneikis** [e], **T. Šalkus** [a], **and A. Kežionis** [a]

[a] *Faculty of Physics, Vilnius University, Saulėtekio 9/3, LT-10222 Vilnius, Lithuania*
E-mail: vilma.venckute@ff.vu.lt

[b] *Department of Material Science and Engineering, National Cheng Kung University, No. 1 University Road, 70101 Tainan, Taiwan*

[c] *Institute of Applied Research, Vilnius University, Saulėtekio 9/3, LT-10222 Vilnius, Lithuania*

[d] *Institute of Inorganic Chemistry, Riga Technical University, Miera 34, 2169 Salaspils, Latvia*

[e] *Semiconductor Physics Institute, Center for Physical Sciences and Technology, A. Goštauto 11, LT-01108 Vilnius, Lithuania*

The powders of LiFePO$_4$ compounds have been synthesized by the solid state reaction, and LiFePO$_4$/C composites were sintered in argon gas. The ceramics of LiFePO$_4$ were sintered in air. The surfaces of the ceramics were investigated by a scanning electron microscope (SEM), energy dispersive X-ray spectrometer (EDX). The binding energies of the Fe 2p, P 2p, and O 1s core level of LiFePO$_4$ ceramic and LiFePO$_4$/C composite surfaces were determined by X-ray photoelectron spectroscopy (XPS). The deconvolutions of Fe 2p core level XPS are associated with Fe^{2+} and Fe^{3+} valence states of the ceramics. Impedance spectroscopy of the ceramics has been performed in the frequency range of 10 Hz to 3 GHz by low frequency and microwave impedance spectrometers. Two- and four-probe methods were used for measurements at low frequencies. The LiFePO$_4$/C composite was investigated in nitrogen gas, and the measurements of LiFePO$_4$ were conducted in air. The measurements of the electrical properties of the ceramics were carried out in the temperature interval of 300–500 K.

Keywords: ceramics, XPS, SEM/EDX, impedance spectroscopy, relaxation dispersion

PACS: 82.45.Xy, 84.37.+q, 79.60.-i

1. Introduction

LiFePO$_4$ is an attractive cathode material for Li ion secondary batteries [1]. Lithium iron phosphate crystallizes in olivine structure and is indexed in orthorhombic symmetry with the Pnma space group [2]. It is known [3] that in this compound Fe^{2+} can oxidize to Fe^{3+}. The compound is a mixed electronic–ionic conductor, and at room temperature the values of electronic and ionic conductivities were found to be 3.7×10^{-7} S/m and 5.0×10^{-3} S/m, respectively [4]. According to [5], the activation energies of electronic and ionic conductivities in the temperature range of 300–660 K were 0.66 and 0.63 eV, respectively. The conductivity values increased by increasing the amount of carbon in the LiFePO$_4$/C composites [6]. There are many publications where conductivity of LiFePO$_4$ was investigated at low frequencies [4–8]. The O 1s, Fe 2p, P 2p core level XPS depends on the sputtering time of LiFePO$_4$ samples by Ar$^+$ [9]. The oxidation process of Fe^{2+} to Fe^{3+} in LiFePO$_4$ causes a chemical shift of 1.2 eV towards a higher binding energy for Fe 2p$_{1/2}$ core level XPS [10]. The redox behaviour of iron and high values of ionic conductivity in this compound make it also an interesting candidate for ionic dynamics study in a broad frequency range of the electric field. XPS, EDX, and impedance spectroscopy investigation results of pure LiFePO$_4$ and carbon containing LiFePO$_4$/C ceramics are presented in this work.

2. Experiments

The powders of pure LiFePO$_4$ have been synthesized by the solid state reaction. The precursors FePO$_4 \cdot 4H_2O$ and LiOH·H$_2$O have been used for the synthesis as the raw materials. Stoichiometric amounts of FePO$_4 \cdot 4H_2O$ and LiOH · H$_2$O were ball-milled for 24 h in ethyl alcohol. After drying the slurry at 353 K, the powder was heated at 1073 K in the argon atmosphere for 4h. The LiFePO$_4$/C composite was prepared

from $FeC_2O_4 \cdot 2H_2O$ (Aldrich Chemical Company, purity 99%), Li_2CO_3 (99.99%), and $(NH_4)_2HPO_4$ (99%). The stoichiometric amounts of precursors were mixed and heated in the argon atmosphere for 1 h at 1073 K. The estimated carbon amount in the $LiFePO_4$/C powder was 3.6 wt.%. Ceramics were sintered for all the measurements. The powder was pressed at 300 MPa. The $LiFePO_4$/C composite was sintered at 1073 K for 1 h in the Ar atmosphere. $LiFePO_4$ ceramics were sintered for 10 h at 1073 K in air. The relative densities of the $LiFePO_4$/C composite and $LiFePO_4$ ceramics were found to be 73.7% (theoretical density $d_t = 3.42$ g/cm³) and 85.8% ($d_t = 3.6$ g/cm³), respectively. The SEM/EDX (TM3000 – *Hitachi*) analyser was used for microstructure analysis and chemical composition determination. Chemical bonding states of the constituent elements of the surfaces of the ceramics were examined by XPS. The XPS spectra were obtained using Al K_α (hν = 1486.6 eV) radiation at an average of 30 scans with a step size of 0.05 eV. The residual pressure in the analyser chamber was $1.3 \cdot 10^{-8}$ Pa. The fitting of the core level data was performed using a nonlinear fitting procedure (software XPSPEAK 41). For the measurements of complex conductivity ($\tilde{\sigma} = \sigma' + i\sigma''$), complex resistivity ($\tilde{\rho} = \rho' - i\rho''$), and complex dielectric permittivity ($\tilde{\varepsilon} = \varepsilon' - i\varepsilon''$) of LiFePO4/C, the sputtered Au electrodes were prepared. For the electrical measurements of $LiFePO_4$ ceramics, electrodes were made from the Pt paste (GWENT Company). Investigation of electrical properties of $LiFePO_4$/C samples was performed in nitrogen gas in the frequency range from 1 Hz to 5 MHz by a two-probe method (Solartron 1260 analyser). Investigation of electrical properties of $LiFePO_4$ was performed in air in the $1–1 \cdot 10^6$ Hz frequency range by two- and four-probe methods (as described in [11]), and the measurements in the frequency range of $3 \cdot 10^5 – 3 \cdot 10^9$ Hz were performed as described in [12].

3. Results and discussion

SEM images of $LiFePO_4$ ceramic and $LiFePO_4$/C composite surfaces are presented in Fig. 1(a, b). The grain sizes in the investigated area of the $LiFePO_4$ ceramic surface vary in the range from approximately 3.1 to 8.5 μm. The $LiFePO_4$/C composite has numerous microcracks. Figure 2(a, b) shows EDX spectra. The results of investigation of the elemental composition of $LiFePO_4$ ceramics have shown a small amount of Al, Na, Ti, and Co impurities (see the insets of Fig. 2(a)). There is a small amount of Al impurities in $LiFePO_4$/C (Fig. 2(b)). Al_2O_3 substrates used for sintering can be an Al impurity source. If the amount of the registered element is up to 1 at.% (Na, Ti, and Co impurities), the
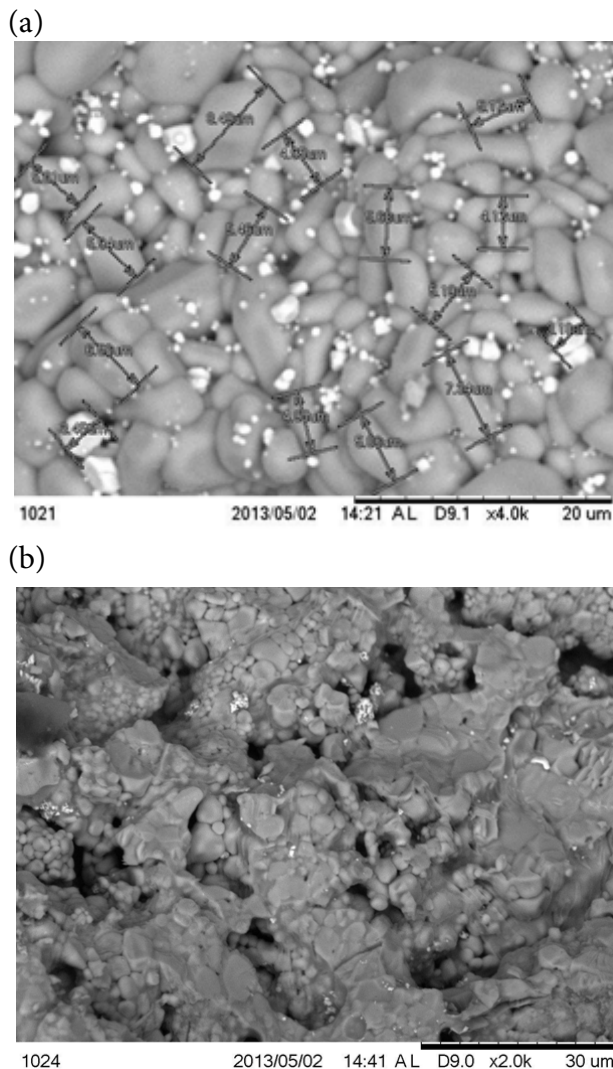
(a)

(b)

Fig. 1. SEM images of (a) $LiFePO_4$ and (b) $LiFePO_4$/C ceramic surfaces.

most probable explanation is the errors of the equipment.

The binding energies in XPS were calibrated by assigning the C 1s peak to 284.6 eV. Fe $2p_{3/2}$, P 2p, and O 1s core level XPS of ceramic $LiFePO_4$ and $LiFePO_4$/C were deconvoluted and their binding energies are presented in Table 1. The XPS of Li 1s cannot be separated from the intensive overlapping Fe 3p peak. The Fe $2p_{3/2}$ XPS of both samples is composed of nine peaks with different binding energies (Fig. 3(a)) as in [13]. The binding energies of Fe 2p peaks were in the range from 709.6 to 718.0 eV and in the range from 709.4 to 717.9 eV in $LiFePO_4$ and $LiFePO_4$/C samples, respectively. Grosvenor et al. assigned Fe $2p_{3/2}$ core level XPS peaks at the binding energies of 710.2, 711.3, 712.4, and 713.6 eV to the Fe^{3+} valence state, and peaks at the binding energies of 708.3, 709.3, and 710.4 eV to the Fe^{2+} valence state in Fe_3O_4 [13]. For $LiFePO_4$ ceramics the Fe 2p peaks at the binding energies of 709.6,
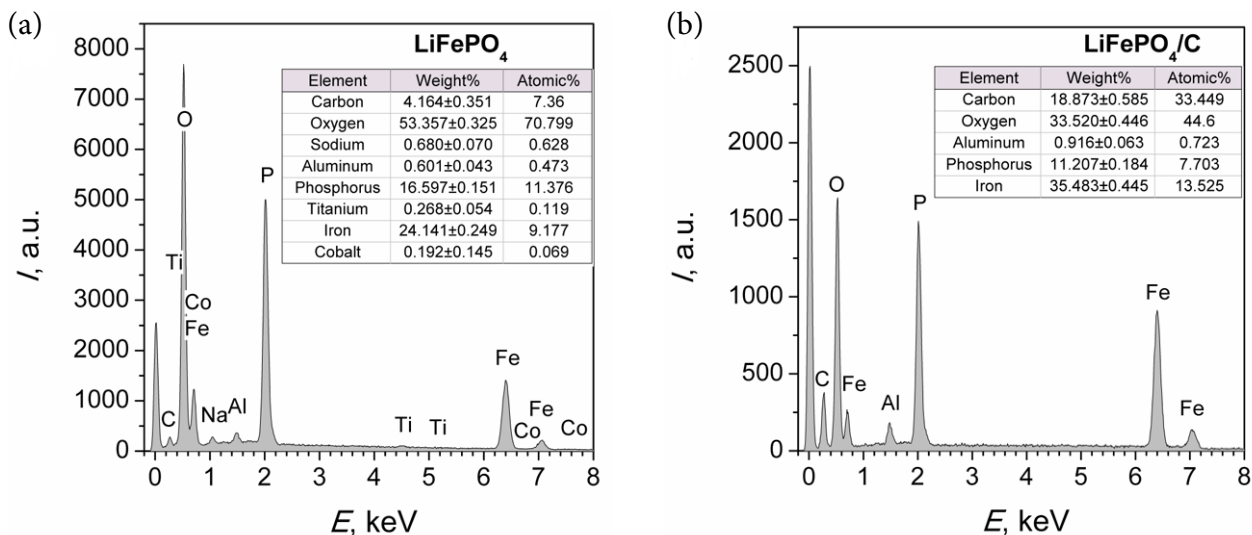
(a)

(b)

Fig. 2. EDX spectra of (a) LiFePO$_4$ and (b) LiFePO$_4$/C ceramics.

Table 1. Binding and splitting energies of Fe 2p, P 2p, O 1s core levels, amounts and chi-square values in LiFePO$_4$ and LiFePO$_4$/C compounds.

Core level XPS	Compound							
	LiFePO$_4$				LiFePO$_4$/C			
	Binding energy, eV	Splitting energy, eV	Amount, at.%	χ^2	Binding energy, eV	Splitting energy, eV	Amount, at.%	χ^2
Fe 2p$_{3/2}$	709.6		4.8 (2+)	0.7	709.4		10.1 (2+)	0.6
	710.4		4.8 (2+)		710.2		11.0 (2+)	
	711.3		6.2 (2+)		711.2		14.9 (2+)	
	711.8		21.1 (3+)		711.6		17.4 (3+)	
	712.6		35.2 (3+)		712.7		25.0 (3+)	
	713.8		17.8 (3+)		713.8		12.9 (3+)	
	714.5		10.1 (3+)		714.6		8.7 (3+)	
	716.1		Sattelite		716.0		Sattelite	
	718.0		Sattelite		717.9		Sattelite	
P 2p	132.2	1	37.8 (3+)	0.6	135.0	1	45.3 (3+)	0.8
	133.1	1	62.2 (5+)		133.2	1	54.7 (5+)	
O 1s	530.4		16.6	1.74	530.9		26.6	2.1
	531.2		59.2		531.9		26.2	
	532.4		24.2		532.9		28.7	
					533.9		18.5	

710.4, and 711.3 eV were related to the Fe^{2+} oxidation state, and for the LiFePO$_4$/C composite the Fe 2p peaks at the binding energies of 709.4, 710.2, and 711.2 eV were related to the Fe^{2+} valence state, too. These values are larger than in oxide Fe$_3$O$_4$ [13] because the shifting of peaks to a higher binding energy is due to the formation of bonds Fe–O–P instead of Fe–O–Fe and electronegativity of phosphorus is higher than that of iron. The amounts of the Fe^{2+} valence state in LiFePO$_4$ and LiFePO$_4$/C were found to be 15.8 and 36.0 at.%, respectively. The peaks caused by the Fe^{2+} valence state are located in the binding energy ranges from 709.6 to

711.3 eV for LiFePO$_4$ and from 709.4 to 711.2 eV for LiFePO$_4$/C compounds. The results summarized in Table 1 show that the oxidation of Fe^{2+} to Fe^{3+} shifts the binding energy region towards to a higher energy and correlates with results published in [10]. The Fe 2p peaks related to the Fe^{3+} oxidation state for LiFePO$_4$ were found in the binding energy range from 711.8 to 714.5 eV and in LiFePO$_4$/C this region was between 711.6 and 714.6 eV. The amounts of the Fe^{3+} valence state in LiFePO$_4$ and LiFePO$_4$/C were 84.2 and 64.0 at.%, respectively. In the investigated compounds iron should be bivalent. The results of XPS investigations
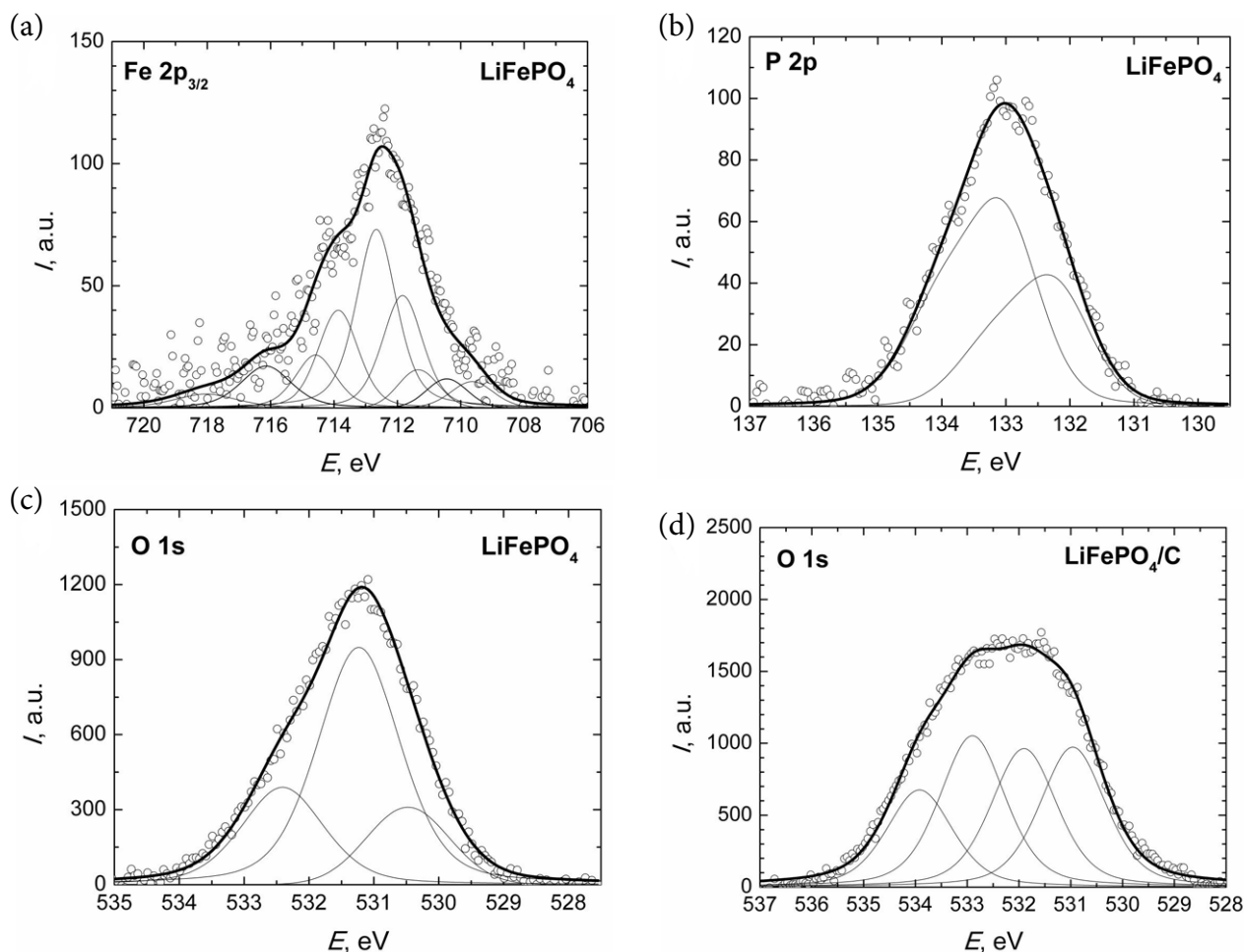
Fig. 3. Characteristic Fe $2p_{3/2}$ (a) and P $2p_{3/2}$ (b) XPS for LiFePO$_4$ and O 1s core level XP spectra of LiFePO$_4$ (c) and LiFePO$_4$/C (d).

showed that the ratio of Fe^{3+}/Fe^{2+} in LiFePO$_4$ and LiFePO$_4$/C was 5.33 and 1.78, respectively. The increase of this ratio in LiFePO$_4$ showed that sintering of the ceramics in air stimulates the reduction of Fe^{2+} into Fe^{3+} valence state. Two Fe 2p satellite peaks are located at the binding energies of 716.1 and 718.0 eV for LiFePO$_4$ and at 716.0 and 717.9 eV for LiFePO$_4$/C. A broad Fe^{2+} satellite peak was found in the compounds with variable compositions such as $Fe^{II}_{6(1-x)}Fe^{III}_{6x}O_{12}H_{2(7-3x)}CO_3 \cdot 3H_2O$ at the binding energy around 715 eV [14].

Each P $2p_{3/2}$ XPS was deconvoluted into two peaks (Fig. 3(b)). The two P 2p peaks in LiFePO$_4$ are at the binding energies of 132.2 and 133.1 eV, which are lower than 133.2 and 135.0 eV binding energies determined for LiFePO$_4$/C (see Table 1). The splitting energies between P $2p_{3/2}$ and P $2p_{1/2}$ core level XPS peaks were 1.0 eV in both compounds. The binding energy of the P 2p peak in compounds with a different structure was found to be 135.6 eV in hexagonal FePO$_4$, 134 eV in orthorhombic LiFePO$_4$ with the olivine-type structure [15], 133.2 eV in LiFePO$_4$ with the pristine structure,

and 133.6 eV in the polymer-LiFePO$_4$ composite [16]. The peak at the binding energy of 133.2 eV in LiFePO$_4$ and the peak at 135.0 eV in LiFePO$_4$/C can be associated with the P^{3+} oxidation state resulting from the $(PO_3)^-$ group as in [17] and other peaks at 133.1 and 133.2 eV (see Table 1) can be associated to the PO_4^{3-} group and attributed to the P^{5+} valence state as in [18].

Figure 3(c, d) shows the O 1s core level XPS of LiFePO$_4$ and LiFePO$_4$/C, respectively. In the LiFePO$_4$ compound the O 1s spectrum has been deconvoluted into three peaks as in [14, 19] but on the LiFePO$_4$/C surface four peaks with different binding energies were detected. The O 1s peak (see Table 1) at the binding energy of 531.2 eV (corresponding amount 59.2 at.%) for LiFePO$_4$ and the peak at the binding energy of 530.9 eV (26.6 at.%) for LiFePO$_4$/C can be attributed to the lattice oxygen O^{2-} bond P–O at the normal sites of the orthorhombic structure, while the other two O 1s peaks at 530.4 and 532.4 eV can be assigned to O^{2-} in the oxidized Fe bond O–Fe and adsorbed OH^-. This result is consistent with results referred for Fe$_2$O$_3$, where

the binding energies of 530.2, 531.5, and 532.5 eV are related to O^{2-}, OH^-, and oxygen in H_2O, respectively [19]. Three peaks of the O 1s core level spectrum recorded on the $LiFePO_4$/C surface at the binding energies of 531.9, 532.9, and 533.9 eV may be originated from carbon oxide groups as CO, CO_2, and CO_3 or H_2O because C 1s XPS has showed a large amount of oxidized carbon related to peaks at 286.1 (29.2 at.%) and 287.7 eV (12.9 at.%) binding energies.

In the present work, the measurements of electrical properties were carried out in the broadband frequency range at different temperatures. Such investigations enable to study ionic transport peculiarities in grain boundaries and grains of the ceramics. The characteristic frequency dependences of the real part of complex conductivity (σ') of the $LiFePO_4$ ceramics measured at different temperatures are showed in Fig. 4. The thermally activated dispersion regions in σ' spectra for both investigated samples were found. The dispersion regions shift towards higher frequencies as temperature increases. This phenomenon is typical of relaxation-type dispersions [20, 21]. The low frequency dispersion regions can be associated with relaxation processes in the grain boundary of the ceramics. The dispersion at high frequencies is caused by ionic transport in the bulk of the ceramics. Grain boundary (f_{gb}) and bulk (f_b) relaxation frequencies were determined from the maxima of the imaginary part of the complex specific resistivity $\rho''(f)$ measured in the investigated frequency range at different temperatures. In Fig. 5, the characteristic frequency dependences of ρ'' at the temperatures of 300, 350, and 400 K of the $LiFePO_4$ compound are shown. The temperature dependences of f_{gb} and f_b for $LiFePO_4$ ceramics and $LiFePO_4$/C composite are presented in Fig. 6. The activation energies ΔE_{fgb} and ΔE_{fb} were calculated from the slopes of the

Fig. 5. Characteristic frequency dependences of imaginary part of complex resistivity at different temperatures of $LiFePO_4$ ceramics.

Fig. 6. Temperature dependences of relaxation frequencies in bulk and grain boundaries of $LiFePO_4$ and $LiFePO_4$/C ceramics.

Arrhenius plots of f_{gb} and f_b. The total conductivities σ_{tot} of the ceramics were derived from the plateaus of $\sigma'(f)$ dependences obtained by the four-probe method at different temperatures, and bulk conductivities σ_b were obtained from complex resistivity plots $\rho''(\rho')$ at different temperatures. The characteristic $\rho''(\rho')$ plots of $LiFePO_4$ ceramics at different temperatures are shown in Fig. 7. The temperature dependences of σ_{tot} and σ_b of the $LiFePO_4$ ceramic and $LiFePO_4$/C composite samples are shown in Fig. 8. The activation energies of σ_{tot} (ΔE_{tot}) and of σ_b (ΔE_b) were found from the slopes of the Arrhenius plots. The experimental results of the investigation of σ_{tot}, σ_b, and their activation energies are summarized in Table 2.

The temperature dependences of dielectric permittivity ε' and dielectric losses $\tan\delta$ were investigated only for $LiFePO_4$ ceramic samples at a 1 GHz
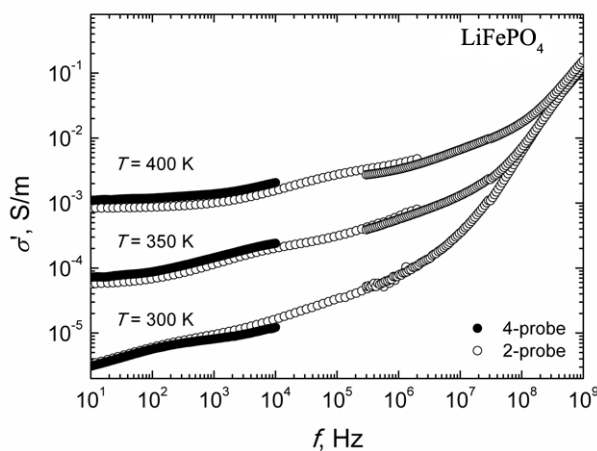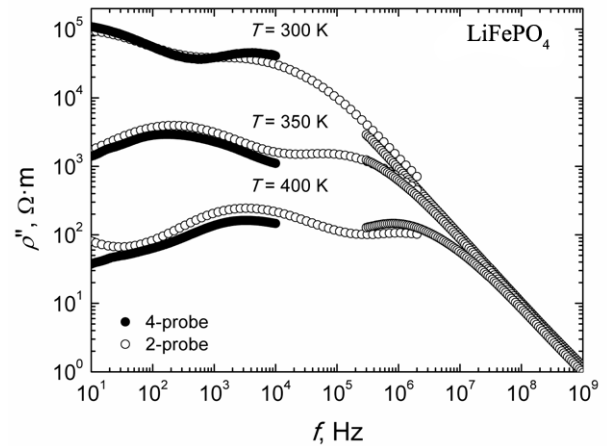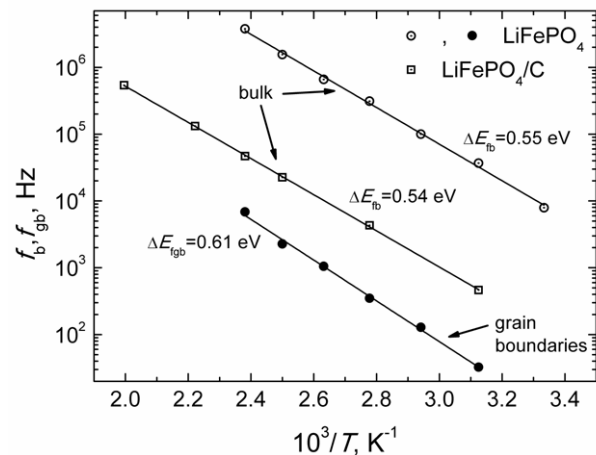

Fig. 4. Characteristic frequency dependences of conductivity of $LiFePO_4$ ceramics at different temperatures.
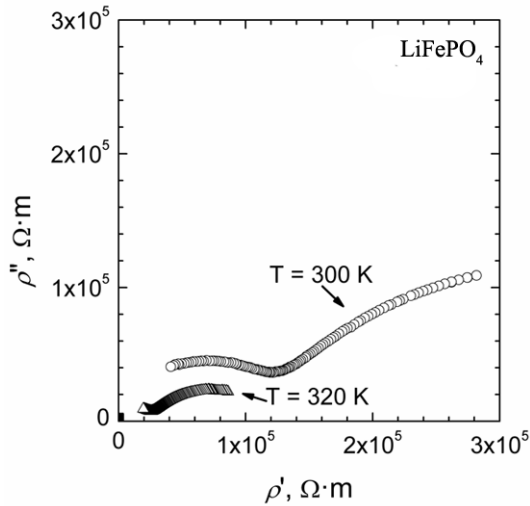
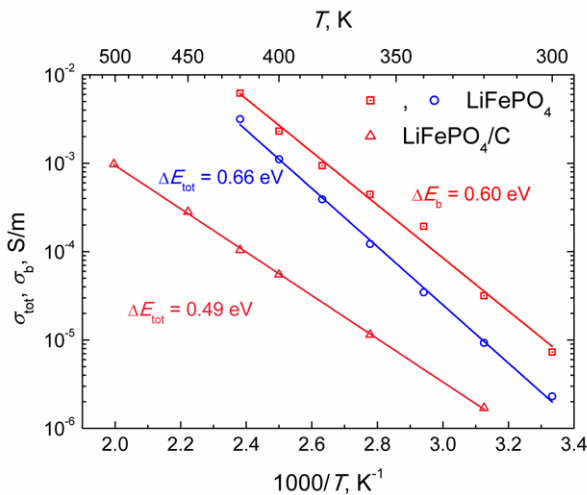Fig. 7. Impedance spectra of LiFePO$_4$ ceramics at different temperatures.

Fig. 8. Temperature dependences of total and bulk conductivities of LiFePO$_4$ and LiFePO$_4$/C ceramics.

frequency. This frequency at 420 K is higher than the Maxwell relaxation frequency:

$$f_M = \sigma_b / 2\pi\varepsilon'\varepsilon_0,$$

where $\varepsilon_0 = 8.85 \cdot 10^{-12}$ F/m is vacuum permittivity. The Maxwell relaxation frequency f_M at 420 K for the

LiFePO$_4$ compound was found to be 5.92 MHz. The temperature dependences of ε' and tanδ of LiFePO$_4$ ceramics are shown in Fig. 9. The values of ε' and tanδ are summarized in Table 2, too. The increase of the ε' values with temperature can be caused by contribution of the migration polarization of lithium ions, vibration of the lattice, and electronic polarization. The increase of the values of tanδ with increase of temperature can be related to the contribution of σ_b.
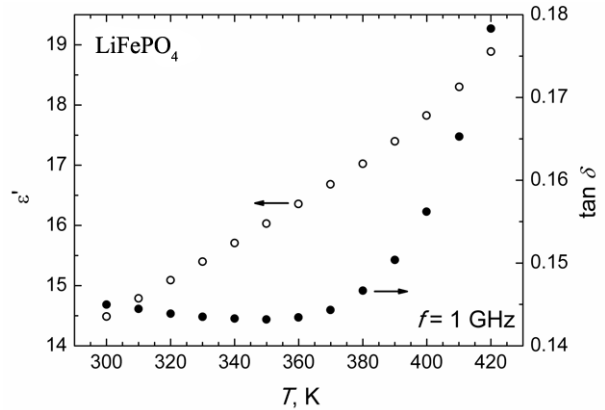

Fig. 9. Temperature dependences of dielectric permittivity and tanδ of LiFePO$_4$ ceramics.

4. Conclusions

The grain sizes of LiFePO$_4$ ceramics sintered in air varied in the range from 3.45 to 7.34 μm. The microstructure of LiFePO$_4$/C composite ceramics sintered in argon gas had numerous microcracks. The results of the investigation of the Fe 2p core level suggest that Fe ions in LiFePO$_4$ and LiFePO$_4$/C are at Fe^{2+} and Fe^{3+} oxidation states. The deconvolution of P 2p XP spectra into two peaks in the investigated ceramics show that the peaks at the binding energy of 133.2 eV in LiFePO$_4$ and the peak at 135.0 eV in LiFePO$_4$/C can be associated with the P^{3+} oxidation state resulting from the (PO$_3$)$^{1-}$ group, and other peaks at 133.1 and 133.2 eV can be associated to the PO$_4$$^{3-}$ group and attributed to the P^{5+} valence state. The O 1s peak at the binding energy of 531.2 eV of LiFePO$_4$ and the peak

Table 2. Summary of electrical characteristic at different temperatures for LiFePO$_4$ and LiFePO$_4$/C samples.

Compound	σ_b, S/m ($T = 320$ K)	ΔE_b, eV	σ_{tot}, S/m ($T = 320$ K)	ΔE_{tot}, eV	ε' (1 GHz) ($T = 320$ K)	tanδ (1 GHz) ($T = 320$ K)	f_M, MHz ($T = 420$ K)	ΔE_{fb}, eV	ΔE_{fgb}, eV
LiFePO$_4$	$3.17 \cdot 10^{-5}$	0.60	$9.3 \cdot 10^{-6}$	0.66	15.09	0.14	5.92	0.55	0.61
LiFePO$_4$/C			$1.65 \cdot 10^{-6}$	0.49				0.54	

at the binding energy of 530.9 eV of $LiFePO_4/C$ can be attributed to the lattice oxygen O^{2-} at the normal sites of the orthorhombic structure, while the other two O 1s peaks can be assigned to OH^- and oxygen in H_2O. The dispersion regions of electrical properties were found, and they were attributed to the relaxation processes related to fast Li^+ ion transport in the grain boundaries and grains of the investigated ceramics. It is shown that relaxation frequencies in grain boundaries and grains increase with temperature according to the Arrhenius law. The values of ε' of the investigated compounds at 1 GHz can be caused by the contribution of the migration polarization of lithium ions, lattice vibrations, and electronic polarization. The values of $\tan\delta$ can be related to the contribution of σ_b in the investigated temperature range.

Acknowledgements

References

[1] Sh.-i. Nishimura, M. Nakamura, R. Natsui, and A. Yamada, New lithium iron pyrophosphate as 3.5 V class cathode material for lithium ion battery, J. Am. Chem. Soc. **132**, 13596–13597 (2010), http://pubs.acs.org/doi/abs/10.1021/ja106297a

[2] C.V. Ramana, A. Mauger, F. Gendron, C.M. Julien, and K. Zaghib, Study of the Li-insertion/extraction process in $LiFePO_4/FePO_4$, J. Power Sources **187**, 555–564 (2009), http://dx.doi.org/10.1016/j.jpowsour.2008.11.042

[3] K. Rissouli, K. Benghouja, J.R. Ramos-Berrado, and C. Julien, Electrical conductivity in lithium orthophosphates, Mater. Sci. Eng. B **98**, 185–189 (2003), http://dx.doi.org/10.1016/S0921-5107(02)00574-3

[4] Ch. Wang and J. Hong, Ionic/electronic conducting characteristics of $LiFePO_4$ cathode materials. The determining factors for high rate performance, Electochem. Solid State Lett. **10**(3), A65–A69 (2007), http://esl.ecsdl.org/content/10/3/A65.abstract

[5] J. Molenda, W. Ojczyk, K. Swierczek, W. Zajac, F. Krok, J. Dygas, and R.-Sh. Liu, Diffusional mechanism of deintercalation in $LiFe_{1-y}Mn_yPO_4$ cathode material, Solid State Ionics **177**, 2617–2624 (2006), http://dx.doi.org/10.1016/j.ssi.2006.03.047

[6] H. Goktepe, H. Sahan, F. Kilic, and S. Patat, Improved of cathode performance of $LiFePO_4/C$ composite using different carboxylic acids as carbon sources for lithium-ion batteries, Ionics **16**, 203–208 (2010), http://dx.doi.org/10.1007/s11581-009-0382-9

[7] R. Amin, Ch. Lin, J. Peng, K. Weichert, T. Acarturk, U. Starke, and J. Maier, Silicon-doped $LiFePO_4$ single crystals: growth, conductivity behavior, and diffusivity, Adv. Funct. Mater. **19**, 1697–1704 (2009), http://dx.doi.org/10.1002/adfm.200801604

[8] L. Wang, H. Wang, Z. Liu, C. Xiao, S. Dong, P. Han, Z. Zhang, X. Zhang, C. Bi, and G. Cui, A facile method of preparing mixed conducting $LiFePO_4/graphene$ composites for lithium-ion batteries, Solid State Ionics **181**, 1685–1689 (2010), http://dx.doi.org/10.1016/j.ssi.2010.09.056

[9] Y.-H. Rho, L.F. Nazar, L. Perry, and D. Ryan, Surface chemistry of $LiFePO_4$ studied by Mössbauer and X-ray photoelectron spectroscopy and its effect on electrochemical properties, J. Electrochem. Soc. **154**(4), A283–A289 (2007), http://jes.ecsdl.org/content/154/4/A283.abstract

[10] M. Manickam, P. Singh, S. Thurgate, and K. Prince, Redox behavior and surface characterization of $LiFePO_4$ in lithium hydroxide electrolyte, J. Power Sources **158**, 646–649 (2006), http://dx.doi.org/10.1016/j.jpowsour.2005.08.059

[11] A. Kežionis, B. Butvilas, T. Šalkus, S. Kazlauskas, D. Petrulionis, T. Žukauskas, E. Kazakevičius, and A.F. Orliukas, Four-electrode impedance spectrometer for investigation of solid ion conductors, Rev. Sci. Instrum. **84**, 013902-8 (2013), http://dx.doi.org/10.1063/1.4774391

[12] A. Kežionis, E. Kazakevičius, T. Šalkus, and A. Orliukas, Broadband high frequency impedance spectrometer with working temperatures up to 1200 K, Solid State Ionics **188**, 110–113 (2011), http://www.sciencedirect.com/science/article/pii/S0167273810005370

[13] A.P. Grosvenor, B.A. Kobe, M.C. Biesinger, and N.S. McIntyre, Investigation of multiplet splitting of Fe 2p XPS spectra and bonding in iron compounds, Surf. Interface Anal. **36**, 1564–1574 (2004), http://dx.doi.org/10.1002/sia.1984

[14] M. Mullet, Y. Guillemin, and C. Ruby, Oxidation and deprotonation of synthetic Fe^{II}–Fe^{III} (oxy)hydroxycarbonate Green Rust: An X-ray photoelectron study, J. Solid State Chem. **181**, 81–89 (2008), http://dx.doi.org/10.1016/j.jssc.2007.10.026

[15] H. Liu, H. Yang, and J. Li, A novel method for preparing $LiFePO_4$ nanorods as a cathode material for lithium-ion power batteries, Electrochimica Acta **55**, 1626–1629 (2010), http://dx.doi.org/10.1016/j.electacta.2009.10.039

[16] H. Mazor, D. Golodnitsky, L. Burstein, A. Gladkich, and E. Peled, Electrophoretic deposition of lithium iron phosphate cathode for thin-film 3D-microbatteries, J. Power Sources **198**, 264–272 (2012), http://dx.doi.org/10.1016/j.jpowsour.2011.09.108

[17] M. Nocun, Structural studies of phosphate glasses with high ionic conductivity, J. Non-Cryst. Solids **333**, 90–94 (2004), http://dx.doi.org/10.1016/j.jnoncrysol.2003.09.047

[18] C.V. Ramana, A. Ait-Salah, S. Utsunomiya, J.-F. Morhange, A. Mauger, F. Gendron, and C.M. Julien, Spectroscopic and chemical imaging analysis of lithium iron triphosphate, J. Phys. Chem. C **111**, 1049–1054 (2007), http://dx.doi.org/10.1021/jp065072c

[19] V. Sieber, H. Hildebrand, S. Virtanen, and P. Schmuki, Investigations on the passivity of iron in borate and phosphate buffers, pH 8.4, Corros. Sci. **48**, 3472–3488 (2006), http://dx.doi.org/10.1016/j.corsci.2005.12.008

[20] W. Bogusz, J.R. Dygas, F. Krok, A. Kezionis, R. Sobiestianskas, E. Kazakevicius, and A. Orliukas, Electrical conductivity dispersion in co-doped NASICON samples, Phys. Status Solidi **183**, 323–330 (2001), http://dx.doi.org/10.1002/1521-396X(200102)183:2<323::AID-PSSA323>3.0.CO;2-6

[21] M. Cretin and P. Fabri, Comparative study of lithium ion conductors in the system $Li_{1+x}Al_xA_{2-x}^{IV}(PO_4)_3$ with A^{IV}=Ti or Ge and $0 \leq x \leq 0.7$ for use as Li^+ sensitive membranes, J. Eur. Ceram. Soc. **19**, 2931–2940 (1999), http://dx.doi.org/10.1016/S0955-2219(99)00055-2

LiFePO$_4$ IR LiFePO$_4$/C KERAMIKŲ SEM/EDX, XPS IR KOMPLEKSINĖS PILNUTINĖS VARŽOS SPEKTROSKOPIJOS TYRIMAI

A.F. Orliukas [a], K.-Z. Fung [b], V. Venckutė [a], V. Kazlauskienė [c], J. Miškinis [c], A. Dindune [d], Z. Kanepe [d], J. Ronis [d], A. Maneikis [e], T. Šalkus [a], A. Kežionis [a]

[a] *Vilniaus universiteto Fizikos fakultetas, Vilnius, Lietuva*
[b] *Nacionalinio Cheng Kung universiteto Medžiagotyros ir inžinerijos fakultetas, Tainanas, Taivanas*
[c] *Vilniaus universiteto Taikomųjų mokslų institutas, Vilnius, Lietuva*
[d] *Rygos technikos universiteto Neorganinės chemijos institutas, Salaspilis, Latvija*
[e] *Fizinių ir technologijos mokslų centro Puslaidininkių fizikos institutas, Vilnius, Lietuva*

Santrauka

LiFePO$_4$ yra gerai žinoma mišraus elektroninio ir joninio laidumų ličio akumuliatorių katodinė medžiaga. Norint padidinti jos elektroninio laidumo sandą yra gaminami LiFePO$_4$ ir anglies kompozitai. Šiame darbe LiFePO$_4$ ir LiFePO$_4$/C junginiai buvo sintezuoti kietųjų fazių reakcijos metodu. LiFePO$_4$/C kompozite buvo nustatytas 3,6 sv.% anglies kiekis. LiFePO$_4$ keramika buvo kepinama ore 1073 K temperatūroje 10 h, o LiFePO$_4$/C kompozitas buvo kepinamas argono atmosferoje 1073 K temperatūroje 1 h. Skenuojančiu elektroniniu mikroskopu (SEM) gautuose LiFePO$_4$ keramikų paviršiaus vaizduose matyti, kad tirtame paviršiaus plote kristalitų dydžiai apytiksliai kinta 3,1–8,5 μm ribose. LiFePO$_4$/C kompozito paviršiuje stebima nemažai mikroįtrūkimų. Rentgeno spindulių dispersijos spektroskopija (EDX) buvo nustatyta, kad LiFePO$_4$ keramikose yra nedidelis Al, Na, Ti ir Co priemaišų kiekis, o LiFePO$_4$/C kompozite nedidelis Al priemaišų kiekis. Keramikų paviršiai buvo tirti Rentgeno fotoelektroninės spektroskopijos metodu. Abiejų medžiagų Fe $2p_{3/2}$ fotoelektronų spektrai buvo aproksimuoti devynių smailių, kurios priskiriamos Fe^{2+} ir Fe^{3+} bei palydovinėms smailėms, superpozicija. Trivalentės geležies kiekiai LiFePO$_4$ ir LiFePO$_4$/C atitinkamai buvo 84,2 ir 64,0 at.%. Abiejuose jungi-

niuose taip pat randama trivalenčio ir penkiavalenčio fosforo. Ličio fotoelektronų spektrai paprastai būna gana silpni, o tirtose medžiagose jie persiklojo su Fe 3p fotoelektronų spektru ir nebuvo galima jų išskirti. Keramikų elektrinės savybės tirtos kompleksinės pilnutės varžos spektroskopijos metodais. LiFePO$_4$/C kompozitas tirtas 1 Hz – 5 MHz dažnių ruože dviejų elektrodų metodu Solartron 1260 pilnutinės varžos analizatoriumi azoto dujų atmosferoje. LiFePO$_4$ matavimai buvo atlikti ore 10 Hz – 2 MHz dažnių ruože dviejų ir keturių elektrodų metodais bei $3 \cdot 10^5$–$3 \cdot 10^9$ Hz dažnių ruože šiems matavimams naudota bendraašė linija. LiFePO$_4$ kompleksinio laidumo realiosios dalies dažninėse priklausomybėse stebimos dvi relaksacinės dispersijos, kurios gali būti siejamos su Li jonų pernaša keramikų tarpkristalitinėse sandūrose (žemi dažniai) bei kristaluose (aukšti dažniai). Tirtuose temperatūrų intervaluose bendrieji keramikų laidumai kinta pagal Arenijaus dėsnį. LiFePO$_4$ keramikos bendrojo laidumo aktyvacijos energija yra 0,60 eV, o LiFePO$_4$/C kompozite – 0,49 eV. Dielektrinės skvarbos realioji dalis buvo tirta 1 GHz dažnio elektriniame lauke 300–420 K temperatūrų intervale. Jos vertės yra nusakomos ličio jonų migracinės poliarizacijos, gardelės virpesių bei elektroninės poliarizacijos indėliais.